

Reliable Computation of Equilibrium States and Bifurcations in Ecological Systems Analysis

C. Ryan Gwaltney and Mark A. Stadtherr*

Department of Chemical and Biomolecular Engineering
University of Notre Dame, Notre Dame, IN 46556, USA

Abstract

A problem of frequent interest in analyzing nonlinear ODE models of ecological systems is the location of equilibrium states and bifurcations. Interval-Newton techniques are explored for identifying, with certainty, all equilibrium states and all codimension-1 and codimension-2 bifurcations of interest within specified model parameter intervals. The methodology is applied to a tritrophic food chain in a chemostat (Canale's model), and a modification of thereof. This modification aids in elucidating the nonlinear effects of introducing a hypothetical contaminant into a food chain.

Keywords: Ecosystem modeling; Ecological risk assessment; Food chains; Equilibrium states; Bifurcations; Nonlinear dynamics

*Author to whom all correspondence should be addressed. Phone: (574) 631-9318; Fax: (574) 631-8366; E-mail: markst@nd.edu

1 Introduction

Ecological systems, including food chains and food webs, are often modeled using systems of nonlinear ordinary differential equations (ODEs). Of particular interest here is the modeling of food chains, which provides challenges in the fields of both theoretical ecology and applied mathematics. Food chain models are descriptive of a wide range of behaviors in the environment, and are useful as a tool to perform ecological risk assessments (Naito et al., 2002). These models are often simple, but display rich mathematical behavior, with varying numbers and stability of equilibria and limit cycles that depend on the model parameters (e.g., Gragnani et al., 1998; Moghadas and Gumel, 2003). Many different model formulations are possible, depending on the number of species analyzed, the predation responses used, whether age or fertility structure is of interest for a given species, and how resources are being modeled for the basal species. Analysis of food chain models is often performed by examining the parameter space of the model in one or more variables. This approach is referred to as bifurcation analysis, and it provides a powerful tool for concisely representing a large amount of information regarding both the number and stability of equilibrium states (steady states) in a model. In a two-parameter bifurcation diagram, the shape of bifurcation curves can elucidate the dependence, or lack thereof, between model parameters, which in turn can provide information on their ecological relevance. Furthermore, both the shape and the order of bifurcation curves in a diagram can be used to make comparisons between different food chain models. We will focus on one particular food chain model here, namely Canale's chemostat model, as described in detail below. We will also develop and study a version of the model that incorporates an ecosystem contaminant.

Determining the equilibrium states and bifurcations of equilibria in a nonlinear dynamical system is often a challenging problem, and great effort can be expended in analyzing even a relatively simple food chain model with nonlinear functional responses. For simple systems, or specific

parts of more complex ones, analytic techniques and isocline analysis may be useful. However, for more complex problems, numerical continuation methods are the predominant computational tools, with packages such as AUTO (Doedel et al., 2002), MATCONT (Dhooge et al., 2003) and others being particularly popular in this context. Continuation methods can be quite reliable, especially in the hands of an experienced user. However, in general, continuation methods are initialization dependent and provide no guarantee that all equilibrium states and all bifurcations of equilibria will be found. Thus, effective use of continuation methods may require some *a priori* understanding of system behavior in order to reliably create an accurate bifurcation diagram. Gwaltney et al. (2004) described an alternative approach, based on interval mathematics, and applied it to a simple tritrophic Rosenzweig-MacArthur model, and variations thereof. We will explore the use of the same approach here, but apply it to more complex models. This computational method uses an interval-Newton approach combined with generalized bisection, and provides a *mathematical and computational guarantee* that *all* equilibrium states and bifurcations of equilibria will be located, without need for initializations or *a priori* insights into system behavior. There are other dynamical features of interest in food chain models, such as limit cycles (and their bifurcations); however, our attention here will be limited to equilibrium states and their bifurcations. Interval methodologies have been successfully applied to the problem of locating equilibrium states and singularities in traditional chemical engineering problems, such as reaction and reactive distillation systems. Examples of these applications are given by Schnepper and Stadtherr (1996), Gehrke and Marquardt (1997), Bischof et al. (2000), and Mönnigmann and Marquardt (2002).

Our interest in ecological modeling is motivated by its use as one tool in studying the impact on the environment of the industrial use of newly discovered materials. Clearly it is preferable to take a proactive, rather than reactive, approach when considering the safety and environmental consequences of using new compounds. Of particular interest is the potential use of room temperature ionic liquid (IL) solvents in place of traditional solvents (Brennecke and Maginn, 2001). IL

solvents have no measurable vapor pressure (i.e., they do not evaporate) and thus, from a safety and environmental viewpoint, have several potential advantages relative to the traditional volatile organic compounds (VOCs) used as solvents, including elimination of hazards due to inhalation, explosion and air pollution. However, ILs are, to varying degrees, soluble in water; thus if they are used industrially on a large scale, their entry into the environment via aqueous waste streams is of concern. The effects of trace levels of ILs in the environment are today not well known and thus must be further studied. Ecological modeling provides a means for studying the impact of such perturbations on a localized environment by focusing not just on single-species toxicity information, but rather on the larger impacts on the food chain and ecosystem. Of course, ecological modeling is just one part of a much larger suite of tools, including toxicological (e.g., Bernot et al., 2005a,b; Ranke et al., 2004; Stepnowski et al., 2004), microbiological (e.g., Docherty and Kulpa, 2005; Pernak et al., 2003) and other (e.g., Gorman-Lewis and Fine, 2004; Ropel et al., 2005) studies, that must be used in addressing this issue.

2 Problem formulation

2.1 Canale’s chemostat model

Canale’s chemostat model is a tritrophic (prey, predator, superpredator) food chain model embedded in a chemostat (a constant volume system, with constant flow in and out). The predator and superpredator grow by consuming the prey and predator species, respectively, while the prey grows by consuming nutrients in the chemostat. The rate at which the prey, predator, and superpredator consume food is modeled by a hyperbolic functional response. The hyperbolic, or Holling Type II, functional response has become the favored way to model feeding rates in theoretical ecology. This type of response is mathematically more complicated than a simple linear response, but provides a leveling-off (saturation) effect that is a more realistic model of behavior observed in

the environment. There is a constant flow through the chemostat, which carries nutrients into the system, and which carries nutrients and organisms out of the system. The model is given by the following balance equations:

$$\frac{dx_0}{dt} = D(x_n - x_0) - \frac{a_1 x_0 x_1}{b_1 + x_0} \quad (1)$$

$$\frac{dx_1}{dt} = x_1 \left[e_1 \frac{a_1 x_0}{b_1 + x_0} - \frac{a_2 x_2}{b_2 + x_1} - d_1 - \varepsilon_1 D \right] \quad (2)$$

$$\frac{dx_2}{dt} = x_2 \left[e_2 \frac{a_2 x_1}{b_2 + x_1} - \frac{a_3 x_3}{b_3 + x_2} - d_2 - \varepsilon_2 D \right] \quad (3)$$

$$\frac{dx_3}{dt} = x_3 \left[e_3 \frac{a_3 x_2}{b_3 + x_2} - d_3 - \varepsilon_3 D \right]. \quad (4)$$

Here x_0 is the nutrient concentration in the system and x_1 , x_2 , and x_3 are the biomasses of the prey, predator, and superpredator populations, respectively. The (nonnegative) parameters a_i , b_i , d_i , and e_i are the maximum predation rate, half-saturation constant, density-dependent death rate, and predation efficiency of the prey ($i = 1$), predator ($i = 2$), and superpredator ($i = 3$) species. The parameter x_n is the nutrient concentration flowing into the system, and the parameter D is the inflow, or dilution, rate (equal to the outflow rate). The term $\varepsilon_i D$ is the density-dependent washout rate of species i . The constant $\varepsilon_i \in [0, 1]$ quantifies how well a species is able to resist washout. For instance, if $\varepsilon_i = 1$, the organism will be unable to resist washout. An example of such a species would be a unicellular algae. Conversely, if $\varepsilon_i = 0$, the organism is completely resistant to washout. Positive terms on the right-hand sides of Eqs. (1–4) represent inflow of nutrient and organism growth. Negative terms represent outflow and consumption of nutrient, and loss of organisms due to predation, wash out, and death. This model has received considerable attention in the field of theoretical ecology (Boer et al., 1998; El-Sheikh and Mahrouf, 2005; Gagnani et al., 1998; Kooi et al., 1997; Kooi, 2003).

As previously stated, our interest in ecological modeling is motivated by its use as a tool for assessing the risk of the industrial use of newly discovered materials, which may enter the

environment as contaminants. Many ecologists recognize that ecosystem modeling is important for estimating risk to ecological systems. However, most current assessment methods rely on examining single species endpoint tests, such as survival, growth and reproductive rates (Pastorok, 2003). Ecological risk estimation using food web models is becoming a more popular method (Bartell et al., 1992, 1999; Lu et al., 2003; Naito et al., 2002, 2003). These methods have aimed at assessing varying toxic effects over varying time scales. Good summaries of current methods are given by Bartell et al. (2003) and Pastorok et al. (2003).

Some popular methods for modeling both lethal and sub-lethal effects utilize a toxic effects factor, which is calculated for each species in comparison to the appropriate experimentally measured toxicological parameters, such as LC_{50} or EC_{50} . The LC_{50} value is the concentration of contaminant at which 50 percent of the organisms in a test sample die over a given period of time. In contrast, the EC_{50} value is the concentration of the contaminant at which 50 percent of the organisms in a test sample are affected in a specific way over a given period of time. The toxic effects factor is interpolated assuming a linear relationship between contaminant concentration and effect. Considering that most exposure-effect curves are concave down up to the LC_{50} or EC_{50} , this method should provide a conservative estimate of risk (Naito et al., 2002).

Here, we will explore a straightforward way of linking the effects of contamination to a food chain model by directly considering the impact of a contaminant on the appropriate model parameters. For instance, one way of modeling the effect of a contaminant on a food chain would be to link the death rate parameters to the LC_{50} values for each species in the model. Thus, an expression for the density dependent death rate d_i could be given by:

$$d_i = d_i^0 + \frac{C}{2C_i^{LC_{50}}} \quad (5)$$

where d_i^0 is the baseline death rate, $C_i^{LC_{50}}$ is the LC_{50} value for species i , and C is the concentration of the contaminant in the system. This sort of model approach would be especially useful when

examining the acutely lethal effect of a contaminant on an organism. However, the sub-lethal effect of a contaminant on other model parameters could be described in a similar manner. Again, up to the LC_{50} value, this method should give a conservative estimate of the potential impact of a contaminant on a food chain or web. This sort of approach does not necessarily account for chronic effects or effects caused by bioaccumulation of compounds. However, measurements to date of octanol-water partition coefficients, for a small number of ILs, suggest that ILs will not tend to bioaccumulate in fatty tissues (Ropel et al., 2005).

2.2 Equilibrium states and bifurcations

The equilibrium (steady-state) condition is simply $\mathbf{f}(\mathbf{x}) = d\mathbf{x}/dt = \mathbf{0}$, which in this case is also subject to the feasibility condition $\mathbf{x} \geq \mathbf{0}$. Here $\mathbf{x} = [x_0, x_1, x_2, x_3]^T$ and $d\mathbf{x}/dt$ is given by Eqs. (1–4). Thus, once all the model parameters have been specified, there is a 4×4 system of nonlinear equations to be solved for the equilibrium states. In general, equation systems of this type, which arise in the modeling of food chains, may have multiple solutions, and the number of equilibrium states may be unknown *a priori*. For simple models it may be possible to solve for many of the equilibrium states analytically, but for more complex models a computational method is needed that is capable of finding, with certainty, all the solutions of the nonlinear equation system. The stability of an equilibrium state can be determined by evaluating the Jacobian matrix $J = d\mathbf{f}/d\mathbf{x}$ at the state and then examining its eigenvalues. According to linear stability analysis, for an equilibrium state to be stable all of the eigenvalues of the Jacobian must have negative real parts.

A bifurcation is a change in the topological type of the phase portrait as one or more model parameters are varied. Bifurcations of interest here occur at parameter values for which the number and/or stability of the equilibrium states changes (Kuznetsov, 1998). We are primarily interested in three types of codimension-one bifurcations, namely fold, transcritical and Hopf, and two types of

codimension-two bifurcations, namely double-fold (or double-zero) and fold-Hopf. The “codimension” of a bifurcation indicates the number of additional conditions required to specify the particular type of bifurcation, and thus the number of parameters that must be allowed to vary. Thus, to find a codimension-one bifurcation, one additional condition must be given, and one parameter (which we denote as α) allowed to vary, and to find a codimension-two bifurcation, two additional conditions must be given, and two parameters (α, β) allowed to vary. Several detailed treatments of bifurcation analysis are available (e.g., Govaerts, 2000; Kuznetsov, 1998; Seydel, 1988).

When a fold or transcritical bifurcation of equilibrium occurs, two equilibria “collide” as the bifurcation parameter is varied. This collision results in either an exchange of stability (transcritical) or mutual annihilation of two equilibria (fold). Mathematically, when an equilibrium state undergoes either a fold or transcritical bifurcation, an eigenvalue of its Jacobian is zero (Govaerts, 2000). Since the determinant of a matrix is equal to the product of its eigenvalues, the determinant of the Jacobian will be zero at a fold or transcritical bifurcation, thereby providing a convenient test function (Kuznetsov, 1998). Thus, to locate fold or transcritical bifurcations of equilibria, the equilibrium condition can be augmented with the additional equation $\det[J(\mathbf{x}, \alpha)] = 0$ and the additional variable α , the bifurcation parameter. The augmented system is then solved to find any fold and transcritical bifurcations, along with the corresponding value or values of α .

When a single equilibrium state changes stability as a model parameter is varied, this corresponds to a Hopf bifurcation. Mathematically, when an equilibrium state undergoes a Hopf bifurcation, its Jacobian has a pair of complex conjugate eigenvalues whose real parts are zero. Thus, there must be a pair of eigenvalues that sums to zero. According to Stephanos’s theorem (Kuznetsov, 1998), for an $n \times n$ matrix J with eigenvalues $\lambda_1, \lambda_2, \dots, \lambda_n$, the bialternate product $J \odot J$ has eigenvalues $\lambda_i \lambda_j$ and the bialternate product $2J \odot I$ has eigenvalues $\lambda_i + \lambda_j$. Thus, to locate a Hopf bifurcation, the equilibrium condition can be augmented (Govaerts, 2000; Kuznetsov, 1998) with the additional equation $\det[2J(\mathbf{x}, \alpha) \odot I] = 0$. The bialternate product of two $n \times n$

matrices A and B is an $m \times m$ matrix denoted by $A \odot B$ whose rows are labeled by the multiindex (p, q) where $p = 2, 3, \dots, n$ and $q = 1, 2, \dots, p-1$, whose columns are labeled by the multiindex (r, s) where $r = 2, 3, \dots, n$ and $s = 1, 2, \dots, r-1$, where $m = n(n-1)/2$, and whose elements are given by

$$(A \odot B)_{(p,q)(r,s)} = \frac{1}{2} \left(\begin{vmatrix} a_{pr} & a_{ps} \\ b_{qr} & b_{qs} \end{vmatrix} + \begin{vmatrix} b_{pr} & b_{ps} \\ a_{qr} & a_{qs} \end{vmatrix} \right). \quad (6)$$

Note that while solutions to the augmented system will include all Hopf bifurcation points, there may be other solutions corresponding to the case of two eigenvalues that are real additive inverses. To identify such “false positives” it is necessary to compute the eigenvalues of the Jacobian at each solution. If the Hopf bifurcation occurs in an independent two-variable subset of state space, this is referred to as a planar Hopf bifurcation. In general, a Hopf bifurcation corresponds to the appearance or disappearance of a limit cycle (stable or unstable) around the equilibrium state (Seydel, 1988). Frequently this corresponds to a change in the stability of the equilibrium state. However, for systems with more than two state variables, this is not always the case, depending on the sign of the real part of other eigenvalues.

The two types of codimension-two bifurcations of interest (double-fold and fold-Hopf) can both be located by using the same augmenting functions as introduced above. When an equilibrium undergoes a double-fold bifurcation, its Jacobian has two zero eigenvalues. When an equilibrium undergoes a fold-Hopf bifurcation, its Jacobian has one eigenvalue that is zero and a pair of purely imaginary complex conjugate eigenvalues. Thus, the determinant of the Jacobian will be zero in both a double-fold and a fold-Hopf bifurcation, because in both cases there is at least one eigenvalue that is zero. Furthermore, in both cases, there is a pair of eigenvalues that will sum to zero, and so the determinant of the bialternate product $2J \odot I$ will be zero. Thus, to locate a double-fold or a fold-Hopf codimension-two bifurcation of equilibrium, the equilibrium condition can be augmented

with the two additional equations $\det[J(\mathbf{x}, \alpha, \beta)] = 0$ and $\det[2J(\mathbf{x}, \alpha, \beta) \odot I] = 0$ and the two additional variables (bifurcation parameters) α and β . The augmented system is then solved to find the codimension-two bifurcations of interest, along with the corresponding values of α and β . Once found, these solutions must be screened for solutions that have a pair of (nonzero) eigenvalues that are purely real additive inverses, and the solutions must be further sorted and classified by type. Codimension-two bifurcations are often of interest since they may serve as “organizing centers” for a two-parameter bifurcation diagram.

Whether one is looking for equilibrium states, or the bifurcations of equilibria discussed above, there is a system of nonlinear equations to be solved that may have multiple solutions, or no solutions, and the number of solutions may be unknown *a priori*. Typically these equation systems are solved using a continuation-based strategy (Kuznetsov, 1998). However, these methods generally offer no guarantee that all equilibrium states or bifurcations will be found, and are often initialization dependent. Bifurcation diagrams can also be generated by using a grid-based approach in which a grid is established in the two-variable parameter space and the number and stability of equilibrium states is computed at each grid point (Fussmann et al., 2000). The resulting information can provide the approximate location of the bifurcation curves on the diagram, but does not give their exact location. A computational method is needed that is capable of finding, with certainty, *all* the solutions of the nonlinear equation systems that characterize equilibrium states and their bifurcations. An interval-Newton methodology is explored here for this purpose.

3 Computational methodology

We provide here a very brief outline of the interval-Newton methodology used. For a more detailed background on interval mathematics, including interval arithmetic, computations with intervals, and interval-Newton methods, there are several good sources available (Hansen and Walster,

2004; Jaulin et al., 2001; Kearfott, 1996; Neumaier, 1990). Additional details of the interval-Newton algorithm used are summarized by Gau and Stadtherr (2002) and Schnepfer and Stadtherr (1996).

Consider an $n \times n$ nonlinear equation system $\mathbf{f}(\mathbf{x}) = \mathbf{0}$ with a finite number of real roots in some initial interval $\mathbf{X}^{(0)}$. The interval-Newton methodology is applied to a sequence of subintervals of the initial interval $\mathbf{X}^{(0)}$; as will be seen below, these subintervals arise in a bisection process. For a subinterval $\mathbf{X}^{(k)}$ in the sequence, the first step is the *function range test*. An interval extension $\mathbf{F}(\mathbf{X}^{(k)})$ of the function $\mathbf{f}(\mathbf{x})$ is calculated, which provides upper and lower bounds on the range of values of $\mathbf{f}(\mathbf{x})$ in $\mathbf{X}^{(k)}$. If there is any component of the interval extension $\mathbf{F}(\mathbf{X}^{(k)})$ that does not include zero, then the interval can be discarded. Additional tools, such as constraint propagation (e.g., Jaulin et al., 2001) or Taylor models (e.g., Makino and Berz, 2003), may also be applied at this point in order to reduce the size of $\mathbf{X}^{(k)}$ or eliminate it.

If it has not been eliminated, the testing of $\mathbf{X}^{(k)}$ continues with the *interval-Newton test*, in which the linear interval equation system

$$F'(\mathbf{X}^{(k)}) \left[\mathbf{N}^{(k)} - \mathbf{x}^{(k)} \right] = -\mathbf{f}(\mathbf{x}^{(k)}) \quad (7)$$

is solved for a new interval $\mathbf{N}^{(k)}$. Here $F'(\mathbf{X}^{(k)})$ is an interval extension of the Jacobian of $\mathbf{f}(\mathbf{x})$ over the interval $\mathbf{X}^{(k)}$, and $\mathbf{x}^{(k)}$ is an arbitrary point in $\mathbf{X}^{(k)}$. It can be shown (Moore, 1966) that any root contained in $\mathbf{X}^{(k)}$ is also contained in the image $\mathbf{N}^{(k)}$. This implies that when $\mathbf{X}^{(k)} \cap \mathbf{N}^{(k)}$ is empty, then no root exists in $\mathbf{X}^{(k)}$, and also suggests the iteration scheme $\mathbf{X}^{(k+1)} = \mathbf{X}^{(k)} \cap \mathbf{N}^{(k)}$. In addition, if $\mathbf{N}^{(k)} \subset \mathbf{X}^{(k)}$, it can be shown (Kearfott, 1996) that there is a unique root contained in $\mathbf{X}^{(k)}$ and thus in $\mathbf{N}^{(k)}$. Thus, after computation of $\mathbf{N}^{(k)}$, there are three possible outcomes: 1. $\mathbf{X}^{(k)} \cap \mathbf{N}^{(k)} = \emptyset$, meaning the current interval $\mathbf{X}^{(k)}$ contains no root, so it can be discarded; 2. $\mathbf{N}^{(k)} \subset \mathbf{X}^{(k)}$, meaning the current interval $\mathbf{X}^{(k)}$ contains a unique root, so it need not be further tested; 3. Neither of the above, but a new interval $\mathbf{X}^{(k+1)} = \mathbf{X}^{(k)} \cap \mathbf{N}^{(k)}$ can be generated. In the last case, if there has been a significant reduction in the size of the interval, then the interval-

Newton test can be reapplied. Otherwise, the interval $\mathbf{X}^{(k+1)}$ is bisected, and the resulting two subintervals are added to the sequence of subintervals to be tested. If an interval containing a unique root has been identified, then this root can be tightly enclosed by continuing the interval-Newton iteration, which will converge quadratically to a desired tolerance. This approach is referred to as an interval-Newton/generalized-bisection (IN/GB) method. At termination, when the subintervals in the sequence have all been tested, either all the real roots of $\mathbf{f}(\mathbf{x}) = \mathbf{0}$ have been tightly enclosed or it has been determined rigorously that no roots exist. An important feature of this approach is that, unlike standard methods for nonlinear equation solving that require a *point* initialization, the IN/GB methodology requires only an initial *interval*.

Using the interval methodology described in this section, it is possible to determine *all* solutions to a nonlinear equation system within a specified initial search interval, or to show that no such solutions exist. This can be done not only with *mathematical certainty*, but also with *computational certainty*, since the use of interval arithmetic with outward rounding eliminates any possible rounding error issues.

4 Results for Canale's model

Following Gragnani et al. (1998), the parameters used were set to $a_1 = 1.25$, $b_1 = 8$, $e_1 = 0.4$, $d_1 = 0.01$, $\varepsilon_1 = 1$, $a_2 = 0.33$, $b_2 = 9$, $e_2 = 0.6$, $d_2 = 0.001$, $\varepsilon_2 = 0.8$, $a_3 = 0.021$, $b_3 = 15.19$, $e_3 = 0.9$, $d_3 = 0.0001$, $\varepsilon_3 = 0.1$. A bifurcation diagram with the inflow rate, D , and the concentration of the nutrient in the inflow, x_n , as the bifurcation parameters was then computed using the IN/GB methodology and compared to the D vs. x_n bifurcation diagram determined by Gragnani et al. (1998) using continuation techniques. The bifurcation diagram for Canale's model computed using IN/GB is given in Fig. 1.

The codimension-one bifurcation curves were computed by solving the appropriate equation

systems (see Section 2.2), first fixing x_n at many (400) closely spaced values over the interval $[0,400]$ and determining the value(s) of D at which bifurcations occurs, and then fixing D at many (700) closely spaced values over the interval $[0,0.14]$ and determining the value(s) of x_n at which bifurcations occurs. The average CPU time required to solve a system for transcritical and fold bifurcations was about 15 seconds (1.7 GHz Xeon processor running Linux) and for Hopf bifurcations about 100 seconds (the many nonlinear systems that must be solved are independent and can be solved in parallel). Some planar Hopf (H_p) bifurcation curves are shown (both in Fig. 1 and in Gragnani et al.'s diagram) for which a stability change occurs only in a two-variable subspace, with the stability of the overall system remaining unchanged (unstable) due to the sign (positive) of the third and/or fourth eigenvalue.

Fig. 1 captures all bifurcations of equilibria shown in the D vs. x_n bifurcation diagram presented by Gragnani et al. (1998). However, we have also located other bifurcation curves not shown by Gragnani et al. (1998). First, we compute a transcritical bifurcation curve very near the D axis (the leftmost TE in Fig. 1) that is not given by Gragnani et al. (1998). At this bifurcation, a stable nutrient-only equilibrium state collides with an infeasible nutrient-prey equilibrium state; the nutrient-prey state becomes feasible and exchanges stability with the nutrient-only state. Second, we compute a planar Hopf bifurcation curve near the x_n axis (lowest H_p in Fig. 1) that is not shown by Gragnani et al. (1998) (we have also computed other planar Hopf bifurcations curves very near the x_n axis, but these are not visible in Fig. 1 due to the scale used). However, for all of these H_p bifurcations, the stability change occurs only in a two-variable subspace, with the stability of the overall system remaining unchanged (unstable).

Another useful type of diagram in nonlinear dynamics is the solution branch diagram (or one-parameter bifurcation diagram). This type of diagram shows how the steady-state values and stability of the state variables change as a single model parameter is varied. These diagrams are also very easily generated using the interval methodology by simply solving the equilibrium conditions.

For example, Fig. 2 shows how the equilibrium states change as the inflow nutrient concentration, x_n , is varied from 0 to 400, while the inflow rate, D , is held constant at a value of 0.09. This was computed by using IN/GB to solve the equilibrium conditions for many (4000) closely spaced values of x_n . The average CPU time to solve for the equilibrium states for one x_n value was about 0.06 seconds. In Fig. 2, and in subsequent solution branch diagrams, thin lines represent unstable equilibria while thick lines represent stable equilibria.

Fig. 2 tracks the behavior of equilibrium states as x_n is increased from 0 to 400 along the horizontal line $D = 0.09$ in Fig. 1. Moving to the right along this line, seven bifurcations are encountered, namely (and in order) TE, TE, H_p, FE, TE, H, H. The first TE is not clearly visible in Fig. 2 due to the scale used. The sixth and seventh bifurcations, both Hopf, are of particular interest here. The sixth bifurcation ($x_n \approx 112.5$) results in the first stable coexisting equilibrium state (all three species present). But at the seventh bifurcation ($x_n \approx 184.5$), this state becomes unstable. This illustrates the “paradox of enrichment”. A minimum inflow nutrient concentration is necessary to support a stable, coexisting state for all three species. Enriching the food chain by increasing the inflow nutrient concentration will increase the stable population of the top predator, but only to a point. Beyond that point (Hopf bifurcation) the system becomes unstable and populations experience “boom and bust” cycles. To directly study the change in system behavior that occurs at this bifurcation (or any of the other bifurcations identified in this study), dynamic simulations can be performed. In this case, dynamic simulations show that, at this Hopf bifurcation, a stable limit cycles appears around the unstable steady state. On this periodic orbit the state variables (mass values or populations) experience “boom and bust” cycles (Gragani et al., 1998).

Using solution branch diagrams like Fig. 2 we can characterize the regions in Fig. 1 and identify the bounds on the region of x_n and D that corresponds to a stable, coexisting steady state. This region is shown by the shaded area in Fig. 1. As indicated in Fig. 1, as the inflow rate, D , increases, the minimum inflow nutrient concentration, x_n , required to support a stable, coexisting

steady state also increases. This behavior is intuitive because, as the inflow rate increases, more nutrient and organisms are washed out of the system, resulting in the need for a higher nutrient inflow concentration, x_n , to support the minimum biomasses of prey and predators necessary for survival of the predators and superpredators, respectively.

The maximum x_n boundary for the region supporting a stable, coexisting steady state is the rightmost Hopf bifurcation curve. At x_n values to the of right this curve, the system is over-enriched and loses stability. One can see from Fig. 1 that at relatively low inflow rates ($D \lesssim 0.0414$), increasing D causes the maximum x_n allowable for a stable coexisting state to decrease. This can be explained by recognizing that at very low values of the inflow rate, D , increasing the inflow rate has the predominant effect of increasing the addition of nutrients to the system, thereby leading to over-enrichment and decreasing the inflow nutrient concentration at which the rightmost Hopf bifurcation occurs in Fig. 2. However, at values of $D \gtrsim 0.0414$, increasing the inflow rate causes the effects of washout to become more pronounced, and larger values of x_n are allowable because of the high removal rate of both biomass and system nutrient.

Using the techniques developed here it is a relatively simple matter to generate bifurcation diagrams in different parameter spaces within the model. Furthermore, generating these diagrams can be done reliably, without need for *a priori* insight and without worry about initialization issues. Here we will next explore bifurcation diagrams for a different model, namely Canale’s model as modified to include the effect of contaminant.

5 Results for Canale’s model with contaminant

Canale’s chemostat model was modified to include the linearly increasing death rate function given by Eq. (5). The baseline death rates d_1^0 , d_2^0 , and d_3^0 were set to the d_1 , d_2 , and d_3 values given above (Gragnani et al., 1998). Various scenarios were studied for the LC_{50} values used for the prey,

predator, and superpredator species. The values chosen were selected to reflect orders of magnitude difference in the sensitivity of each species to the hypothetical contaminant. The values used were combinations of $C_i^{\text{LC}_{50}}$ set to 10, 100, and 1000, used once for each species. There were six possible combinations of these values, and six figures, each a C vs. x_n bifurcation diagram generated using IN/GB as described above, were generated. These cases are organized for discussion into three sections, depending on which species is most sensitive to the contaminant.

5.1 Prey most sensitive

Fig. 3 shows the case where the contaminant is most lethal to the prey trophic level ($i = 1$). The diagram on the left shows the case where the contaminant is least lethal to the superpredators ($C_1^{\text{LC}_{50}} = 10$, $C_2^{\text{LC}_{50}} = 100$, $C_3^{\text{LC}_{50}} = 1000$), while the diagram on the right shows the case where the contaminant is least lethal to the predators ($C_1^{\text{LC}_{50}} = 10$, $C_2^{\text{LC}_{50}} = 1000$, $C_3^{\text{LC}_{50}} = 100$).

Both diagrams in Fig. 3 exhibit transcritical, fold, Hopf, and planar Hopf codimension-one bifurcations, and each diagram has a single codimension-two fold-Hopf bifurcation. Both diagrams were generated on a 3.2 GHz Pentium IV processor running the Intel Fortran Compiler 7.1 for Linux. The average CPU time necessary to solve for fold and transcritical bifurcations was 3.2 seconds for the diagram on the left and 2.2 seconds for the diagram on the right. The average CPU time necessary to compute Hopf bifurcations was 16.6 seconds for the diagram on the left and 10.9 seconds for the diagram on the right. The time necessary to solve for the fold-Hopf codimension-two bifurcation point was 454 seconds for the diagram on the left and 266 seconds for the diagram on the right.

A solution branch diagram was computed for each toxicity case examined in Fig. 3. While the solution branch diagrams were not quantitatively identical, the general qualitative trends can be captured by a single diagram. Fig. 4 is a solution branch diagram that illustrates the effect of increasing the contaminant concentration for the case $C_1^{\text{LC}_{50}} = 10$, $C_2^{\text{LC}_{50}} = 100$, and $C_3^{\text{LC}_{50}} = 1000$

(Fig. 3, left), with $x_n = 200$ and $D = 0.07$. This figure aids in the characterization of the different regions in Fig. 3. Furthermore, Fig. 4 gives insight into the behavior of the system under increasing contaminant loads. As the contaminant level in the system increases, the system transitions from an unstable, likely cyclical, state to a stable, coexisting steady state in a Hopf bifurcation at $C \approx 1.21$. Over the range of stability of this coexisting equilibrium state, increasing the contaminant concentration has the expected effect of reducing the steady-state prey population. However, simultaneously, the steady-state predator population increases, while the superpredator population decreases. The behavior is somewhat unexpected. Since the superpredator population is least sensitive to the hypothetical toxin, one might intuitively expect that contaminating the system would have the least effect on the superpredator. Furthermore, with declining steady-state prey populations, one would expect that the predator population would decline as well. However, from another point of view, the behavior of this system appears reasonable. Since the superpredator is the top species in the food chain, effects to species below the superpredator will directly affect the superpredator population. Declining steady-state superpredator populations reduce predation pressures on the middle trophic level, allowing the predators to flourish. This, in turn, increases predation pressure on the prey trophic level, compounding the effects of the high sensitivity to the ecotoxin and causing the prey population to decrease.

In Fig. 3, the scales of the two diagrams are different in terms of the range of contaminant concentration examined. The contaminant concentration for the diagram on the left ranges from 0 to 10, while on the right the range is from 0 to 2. This disparity in scaling was chosen to highlight the difference between the diagrams in terms of the behavior of the fold, transcritical, and Hopf bifurcation curves to the right and/or below the planar Hopf bifurcation. While this set of curves appears virtually identical between the two diagrams, it is worth noting the difference in the scaling. Furthermore, if the scale of the diagram on the right was increased to match the diagram on the left, the leftmost transcritical curve on both diagrams would match identically. This curve forms

the boundary at which the nutrient-only state collides with the nutrient-prey state, and occurs when $x_2 = 0$ and $x_3 = 0$. To the right of this curve, the nutrient-prey state is feasible. Since $C_1^{\text{LC}_{50}} = 10$ in both diagrams, mathematically this line should be identical. However, moving left to right in both diagrams, the next transcritical bifurcation observed is not identical. This curve forms the boundary at which a nutrient-prey-predator system becomes feasible. The shape of this transcritical bifurcation in both diagrams is very similar, but concavity of the curve is much greater for the system in which the predator is least sensitive to the contaminant ($C_2^{\text{LC}_{50}} = 1000$). Thus, the sensitivity of the predator species, as expected, determines to what extent the predator species in a nutrient-prey-predator state can tolerate the ecotoxin.

Of particular interest in Fig. 3 is the region in which all three species can coexist. This region is shaded grey in both diagrams. The regions themselves display virtually identical trends in terms of the relationship between inflow nutrient concentration, x_n , and contaminant concentration, C . The shape of these regions generally indicates that, by increasing the inflow nutrient concentration, the system will be able to tolerate higher contaminant concentrations as compared to a system that is not enriched. The difference between the two diagrams in Fig. 3 gives the reader information concerning the sensitivity of the system to contaminant. In the diagram on the right, for which the predator is least sensitive ($C_2^{\text{LC}_{50}} = 1000$), the maximum allowable contaminant concentration for coexistence is $C \approx 1.03$ at $x_n = 400$. In the diagram on the left, for which the superpredator is least sensitive ($C_3^{\text{LC}_{50}} = 1000$), the maximum allowable contaminant concentration for coexistence is $C \approx 4.02$ at $x_n = 400$. This difference between the two scenarios indicates that the superpredator plays an important role in the top-down control of the food chain.

5.2 Predator most sensitive

The next pair of systems examined are those in which the predator ($i = 2$) is species most sensitive to contamination, and the results for these systems are shown in Fig. 5. The diagram on

the left shows the case where the contaminant is least lethal to the superpredators ($C_1^{LC_{50}} = 100$, $C_2^{LC_{50}} = 10$, $C_3^{LC_{50}} = 1000$), while the diagram on the right shows the case where the contaminant is least lethal to the prey ($C_1^{LC_{50}} = 1000$, $C_2^{LC_{50}} = 10$, $C_3^{LC_{50}} = 100$).

Notice first that the two diagrams in Fig. 5 differ in the types of bifurcations present. The diagram on the right exhibits transcritical, fold, Hopf, planar Hopf, and fold-Hopf bifurcations, while the diagram on the left does not display any fold or fold-Hopf bifurcations. The diagram on the left was generated using a 3.2GHz Pentium IV processor while the diagram on the right was generated using a 1.7GHz Xeon processor. Both were generated using the Intel Fortran Compiler 7.1 for Linux. The average CPU time necessary to solve for fold and transcritical bifurcations was 1.5 seconds for the diagram on the left and 9.72 seconds for the diagram on the right. The average CPU time necessary to compute Hopf bifurcations was 9.15 seconds for the diagram on the left and 41.4 seconds for the diagram on the right. The time necessary to solve for the fold-Hopf codimension-two bifurcation point was 2502 seconds for the diagram on the right, and it took 318 seconds to show that no codimension-two fold-fold or fold-Hopf points existed for the diagram on the left. The differences between the computation times for the two diagrams are clearly due in part to the difference in the CPUs used.

As done previously, solution branch diagrams were generated for both cases examined in Fig. 5. The two diagrams were not quantitatively or qualitatively identical. However, the general trends are quite similar with a few exceptions, which can be noted by the different order and types of bifurcation curves encountered in the two diagrams in Fig. 5. Thus, only one solution branch diagram is presented here. Fig. 6 is a solution branch diagram that illustrates the effect of increasing the contaminant concentration for the case $C_1^{LC_{50}} = 1000$, $C_2^{LC_{50}} = 10$, and $C_3^{LC_{50}} = 100$ (Fig. 5, right), with $x_n = 200$ and $D = 0.07$. If Fig. 6 was generated for the system on the left in Fig. 5, the main difference would be that the stable, coexisting steady state would not lose stability in a Hopf bifurcation. Rather, the stable coexisting state would cease to exist in a transcritical

bifurcation. Furthermore, the planar Hopf bifurcation would have no effect on system stability, and no fold bifurcations would be observed. However, it is important to note that the general trends observed for the steady-state biomasses for the three species are qualitatively similar when increasing the contaminant concentration. As the contaminant concentration increases, the system transitions to a stable, coexisting steady state. This occurs because the contaminant increases the death rates of the species, causing unstable population cycles to dampen and collapse in a Hopf bifurcation at $C \approx 0.269$. Over the range of stability of this coexisting equilibrium state, increasing the contaminant concentration has an unexpected effect. The superpredator and prey populations both decrease while the predator population increases, despite the fact that the predator species is the most sensitive to the contaminant. This behavior is obviously counterintuitive, but is once again indicative of the top-down control of the food chain by the superpredator species.

The region of stable coexistence for the three species is shaded grey for both diagrams in Fig. 5. In the left diagram in Fig. 5, the lower bound of the region is defined by the Hopf bifurcation, while the upper bound is defined by the rightmost transcritical bifurcation. In the right diagram, the lower and upper bounds on the region of stable coexistence are defined by the Hopf bifurcation curves. The same general trend for the region of stable coexistence is observed in the diagrams in Fig. 5 as was observed in the diagrams in Fig. 3. That is, as the inflow nutrient concentration, x_n , increases, the maximum allowable contaminant concentration, C , for stable coexistence of the food chain also increases. Furthermore, as in Fig. 3, the coexisting steady state is more tolerant to higher contaminant concentrations in the system where the superpredator is least sensitive to the ecotoxin. This is readily apparent by observing that the upper bound on the contaminant concentration is $C \approx 1.17$ for the right diagram, where the superpredator is moderately sensitive ($C_3^{LC_{50}} = 100$), while the upper bound is $C \approx 2.43$ for the left diagram, where the superpredator is least sensitive ($C_3^{LC_{50}} = 1000$).

One last feature worth mentioning in Fig. 5 is the difference between the leftmost transcritical

bifurcation curve in each diagram. This curve separates the region of feasibility for the nutrient-only state from the region in which there is both a nutrient-only state and a nutrient-prey state. Each transcritical bifurcation curve displays the same behavior qualitatively for large values of C in that both proceed upwards, then curve to the right and begin to level off, much like the same curves in the diagrams in Fig. 3. However, in the left diagram, this transcritical curve levels off around a value of $C \approx 80$, while in the right diagram this curve levels off around $C \approx 800$. This difference is expected, considering the order of magnitude difference in $C_1^{\text{LC}_{50}}$ between the two diagrams in Fig. 5, and the simplicity of the state space in which this bifurcation occurs. So, while the superpredator exerts top-down control on the limits of the stable, coexisting steady state, the toxicity of the contaminant to the prey species determines the boundary between existence and extinction for the prey species in the nutrient-prey state.

5.3 Superpredator most sensitive

The last set of bifurcation diagrams for Canale's model with a hypothetical contaminant was generated for the systems in which the superpredator ($i = 3$) is the species most sensitive to the ecotoxin ($C_3^{\text{LC}_{50}} = 10$). These systems are shown in Figs. 7 and 8. Fig. 7 shows the bifurcations found at relatively large values of C , and Fig. 8 shows the bifurcations found at relatively small values of C . Fig. 7 is a side-by-side comparison of the two diagrams for the purpose of analyzing the differences in scale of the effect of C on the nutrient-prey state and the nutrient-prey-predator state. The diagram on the left shows the case where the contaminant is least lethal to the prey ($C_1^{\text{LC}_{50}} = 1000$, $C_2^{\text{LC}_{50}} = 100$, $C_3^{\text{LC}_{50}} = 10$), while the diagram on the right shows the case where the contaminant is least lethal to the predators ($C_1^{\text{LC}_{50}} = 100$, $C_2^{\text{LC}_{50}} = 1000$, $C_3^{\text{LC}_{50}} = 10$). To observe the behavior of the bifurcations controlling the stable, coexisting steady state, the diagrams must be significantly rescaled to show only small values of C . When the left diagram is rescaled, the result is the diagram shown in Fig. 8. When the right diagram is rescaled, it is virtually

indistinguishable from Fig. 8, and so only the one diagram is given.

Generation of the diagrams in Fig. 7 and Fig. 8 took place on a 3.2GHz Pentium IV processor using the Intel Fortran Compiler 7.1 for Linux. For the diagram on the left in Fig. 7 (and for Fig. 8), locating fold and transcritical bifurcations took an average of 1.3 seconds of CPU time, while Hopf bifurcations took an average of 9.1 seconds, and the fold-Hopf codimension-two point took 169 seconds. For the right diagram in Fig. 7, locating fold and transcritical bifurcations took an average of 1.5 seconds of CPU time, while Hopf bifurcations took an average of 9.8 seconds, and the fold-Hopf codimension-two point took 161 seconds.

Fig. 7 illustrates the scaling differences between the two systems. In the diagram on the left, where the prey is least sensitive to the ecotoxin and the predator is moderately sensitive, the leftmost transcritical bifurcation is almost vertical. Were the scale extended along the C axis, one would observe that this transcritical bifurcation curves to the left and levels off near $C \approx 800$. In the diagram on the right in Fig. 7, where the predator is least sensitive to the ecotoxin and the prey is moderately sensitive, it is clear that, qualitatively, the same behavior is observed for the equivalent bifurcation curve, with the exception that this curve now levels off near $C \approx 80$. This is the same behavior observed in the equivalent bifurcation curves in Fig. 5, and occurs for the same reason discussed in Section 5.2. The remaining bifurcation curves viewable in the scale of Fig. 7 are a transcritical bifurcation, and a planar Hopf bifurcation. Crossing the planar Hopf curve causes the nutrient-prey-predator state to become stable with increasing contaminant concentration C . By further increasing C and crossing the transcritical bifurcation, the nutrient-prey-predator state becomes infeasible. Since both of these curves define behavior for the predator trophic level, it is clear why there should be quantitative differences between the two cases shown in Fig. 7.

Fig. 8 is a magnification of the diagram on the left in Fig. 7 ($C_1^{\text{LC}_{50}} = 1000$, $C_2^{\text{LC}_{50}} = 100$, $C_3^{\text{LC}_{50}} = 10$). In this system, the prey is least sensitive to the contaminant, and the superpredators are most sensitive. Fig. 8 shows the region of the stable, coexisting steady state. As previously

observed, increasing the nutrient inflow concentration, x_n , increases the maximum allowable contaminant concentration, C , prior to the coexisting state becoming unstable. In comparison to the diagrams in Fig. 3 and Fig. 5, the region of stable coexistence shown in Fig. 8 is highly sensitive to the concentration of the hypothetical contaminant. In fact, the system in Fig. 8 is approximately an order of magnitude more sensitive than the most sensitive system previously studied. This further illustrates the importance of the superpredator on the behavior in the coexisting steady state.

A solution branch diagram was generated for the system shown in Fig. 8. This diagram illustrates the effect of increasing the contaminant concentration, C , on the various feasible steady states, with $x_n = 200$ and $D = 0.07$. This diagram appears as Fig. 9. The qualitative behavior shown in this diagram is very similar to the behavior observed for other systems. As the contaminant concentration increases, the coexisting state first becomes stable in a Hopf bifurcation. A subsequent Hopf bifurcation causes the coexisting state to lose stability. However, increasing the contaminant concentration, C , over the interval where the system is stable causes a decline in the superpredator and prey populations, while the predator population increases.

While the specific scenarios of contamination cause the various systems examined here to display different quantitative behaviors, the qualitative behavior of all the contamination scenarios is strikingly similar. A common theme in theoretical ecology is that when species at the base of a food chain are affected by some change in the system, the top species will be indirectly impacted. This theme is readily apparent in the “paradox of enrichment”, and can also be seen by examining the various contamination scenarios presented here. Furthermore, it is clear that the superpredator species plays an important role in the top-down control of the stable, coexisting steady state in the food chain. Considering the magnitude of the baseline death rate parameter values used ($d_1^0 = 0.01$, $d_2^0 = 0.001$, $d_3^0 = 0.0001$), we would expect the superpredator species to be most sensitive to small changes in the death rate. However, consider the case (Fig. 5, left) in which the superpredators

are two orders of magnitude less sensitive to the contaminant than the predators. In this case, the predators should be more sensitive to the contaminant than the superpredators. However, even in this case, for the stable coexisting steady-state, increasing the contaminant concentration causes a decline in the superpredator population and an increase in the predator population. The predator population does not begin to decline until levels of contaminant are reached at which the superpredators are decimated. This sort of behavior can be quite counterintuitive, but is not uncommon in nonlinear food chain and food web systems.

6 Concluding remarks

We have demonstrated here the utility of an interval-Newton approach for the computationally rigorous and reliable computation of all equilibrium states and bifurcations of equilibria (fold, transcritical, Hopf, double-fold and fold-Hopf) in nonlinear models of ecosystem dynamics, with focus on a model that includes the effect of a contaminant. Using this methodology one can easily, without any need for initialization or *a priori* insight into system behavior, generate complete solution branch and bifurcation diagrams. The ability to easily and reliably analyze nonlinear food chain models can expose unexpected and counterintuitive behavior. The knowledge provided by this sort of analysis may be quite useful in managing risk in the complex and highly interdependent nonlinear systems found in our environment.

7 Acknowledgments

This work was supported in part by the Department of Education Graduate Assistance in Areas of National Needs (GAANN) Program under Grant #P200A010448, by the State of Indiana 21st Century Research and Technology Fund under Grant #909010455 and by the National Oceanic and Atmospheric Administration under Grant #NA050AR4601153.

References

- Bartell, S., Gardner, R., and O'Neill, R. (1992). *Ecological Risk Estimation*. Ann Arbor, MI: Lewis Publishers.
- Bartell, S., Lefebvre, G., Kaminski, G., Carreau, M., and Campbell, K.R. (1999). An ecosystem model for assessing ecological risks in Quebec rivers, lakes, and reservoirs. *Ecological Modelling*, 124, 43–67.
- Bartell, S., Pastorok, R., Akcakaya, H.R., Regan, H., Ferson, S. and Mackay, C. (2003). Realism and Relevance of Ecological Models Used in Chemical Risk Assessment. *Human and Ecological Risk Assessment*, 9, 907–938.
- Bernot, R.J., Kennedy, E.E., and Lamberti, G.A. (2005). Effects of ionic liquids on the survival, movement, and feeding behavior of the freshwater snail, *Physa acuta*. *Environmental Toxicology and Chemistry*, 24, 1759–1765.
- Bernot, R.J., Brueseke, M.A., Evans-White, M.A., and Lamberti, G.A. (2005). Acute and chronic toxicity of imidazolium-based ionic liquids on *Daphnia magna*. *Environmental Toxicology and Chemistry*, 24, 87–92.
- Bischof, C.H., Lang, B., Marquardt, W., and Mönnigmann, M. (2000). Verified determination of singularities in chemical processes. Proc. SCAN 2000, 9th GAMM-IMACS International Symposium on Scientific Computing, Computer Arithmetic, and Validated Numerics, Sept. 18–22, 2000, Karlsruhe, Germany.
- Boer, M.P., Kooi, B.W., and Kooijman, S.A.L.M. (1998). Food chain dynamics in the chemostat. *Mathematical Biosciences*, 150, 43–62.

- Brennecke, J.F. and Maginn, E.J. (2001). Ionic Liquids: Innovative Fluids for Chemical Processing. *AIChE Journal*, 47, 2384–2389.
- Dhooge, A., Govaerts, W. and Kuznetsov, Y.A. (2003). MATCONT: A MATLAB package for numerical bifurcation analysis of ODEs. *ACM Transactions on Mathematical Software*, 29, 141–164.
- Docherty, K.M. and Kulpa, C.F. (2005). Toxicity and antimicrobial activity of imidazolium and pyridinium ionic liquids. *Green Chemistry*, 7, 185–189.
- Doedel, E.J., Paffenroth, R.C., Champneys, A.R., Fairgrieve, T.F., Kuznetsov, Y.A., Oldeman, B.E. and Sandstede, B. (2002). AUTO 2000: Continuation and bifurcation software for ordinary differential equations (with HomCont). User’s Guide. Available with software at <http://sourceforge.net/projects/auto2000>.
- El-Sheikh, M.M.A. and Mahrouf, S.A.A. (2005). Stability and Bifurcation of a Simple Food Chain in a Chemostat with Removal Rates. *Chaos, Solitons and Fractals*, 23, 1475–1489.
- Fussmann, G.F., Ellner, S.P., Shertzer, K.W., and Hairston, N.G. (2000). Crossing the Hopf Bifurcation in a Live Predator-Prey System. *Science*, 290, 1358–1360.
- Gau, C.-Y. and Stadtherr, M.A. (2002). New Interval Methodologies for Reliable Chemical Process Modeling. *Computers and Chemical Engineering*, 26, 827–840.
- Gehrke, V., and Marquardt, W. (1997). A Singularity Theory Approach to the Study of Reactive Distillation. *Computers and Chemical Engineering*, 21 (Suppl.), S1001–S1006.
- Gorman-Lewis, D.J., and Fein, J.B. (2004). Experimental study of the adsorption of an ionic liquid onto bacterial and mineral surfaces. *Environmental Science and Technology*, 38, 2491–2495.

- Govaerts, W.J.F. (2000). *Numerical Methods for Bifurcations of Dynamical Equilibria*. Philadelphia: SIAM.
- Gragnani, A., De Feo, O., and Rinaldi, S. (1998). Food Chains in the Chemostat: Relationships between Mean Yield and Complex Dynamics. *Bulletin of Mathematical Biology*, 60, 703–719.
- Gwaltney, C.R., Styczynski, M.P., and Stadtherr, M.A. (2004). Reliable Computation of Equilibrium States and Bifurcations in Food Chain Models. *Computers and Chemical Engineering*, 28, 1981–1996.
- Hansen, E.R. and Walster, G.W. (2004). *Global Optimization Using Interval Analysis*. New York: Marcel Dekker.
- Kearfott, R.B. (1996). *Rigorous Global Search: Continuous Problems*. Dordrecht, The Netherlands: Kluwer.
- Kooi, B.W., Boer, M.P., and Kooijman, S.A.L.M. (1997). Complex Dynamic Behavior of Autonomous Microbial Food Chains. *Journal of Mathematical Biology*, 36, 24–40.
- Kooi, B.W. (2003). Numerical Bifurcation Analysis of Ecosystems in a Spatially Homogeneous Environment. *Acta Biotheoretica*, 51, 189–222.
- Kuznetsov, Y.A. (1998). *Elements of Applied Bifurcation Theory*. New York: Springer-Verlag.
- Jaulin, L., Kieffer, M., Didrit, O., and Walter, É. (2001). *Applied Interval Analysis*. London: Springer-Verlag.
- Lu, H., Axe, L., and Tyson, T. (2003). Development and application of computer simulation tools for ecological risk assessment. *Environmental Modeling and Assessment*, 8, 311–322.
- Makino, K., and Berz, M. (2003). Taylor models and other validated functional inclusion methods. *International Journal of Pure and Applied Mathematics*, 4, 379–456.

- Moghadas, S.M. and Gumel, A.B. (2003). Dynamical and Numerical Analysis of a Generalized Food-Chain Model. *Applied Mathematics and Computation*, 142, 35–49.
- Mönnigmann, M., and Marquardt, W. (2002). Normal Vectors on Manifolds of Critical Points for Parametric Robustness of Equilibrium Solutions of ODE Systems. *Journal of Nonlinear Science*, 12, 85–112.
- Moore, R.E. (1996). *Interval Analysis*. Englewood Cliffs, NJ: Prentice-Hall.
- Naito, W., Miyamoto, K., Nakanishi, J., Masunaga, S. and Bartell, S. (2002). Application of an Ecosystem Model for Aquatic Ecological Risk Assessment of Chemicals for a Japanese Lake. *Water Research*, 36, 1–14.
- Naito, W., Miyamoto, K., Nakanishi, J., Masunaga, S. and Bartell, S. (2003). Evaluation of an ecosystem model in ecological risk assessment of chemicals. *Chemosphere*, 53, 363–375.
- Neumaier, A. (1990). *Interval Methods for Systems of Equations*. Cambridge, U.K.: Cambridge Univ. Press.
- Pastorok, R., Akcakaya, H.R., Regan, H., Ferson, S. and Bartell, S. (2003). Role of Ecological Modeling in Risk Assessment. *Human and Ecological Risk Assessment*, 9(4), 939–972.
- Pastorok, R. (2003). Introduction: Improving Chemical Risk Assessments through Ecological Modeling. *Human and Ecological Risk Assessment*, 9(4), 885–888.
- Pernak, J., Sobaszekiewicz, K., and Mirska, I. (2003). Anti-microbial activities of ionic liquids. *Green Chemistry*, 5, 52–56.
- Ranke, J., Molter, K., Stock, F., Bottin-Weber, U., Poczebott, J., Hoffmann, J., Ondruschka, B., Filser, J., and Jastorff, B. (2004). Biological effects of imidazolium ionic liquids with varying chain

- lengths in acute *Vibrio fischeri* and WST-1 cell viability assays. *Ecotoxicology and Environmental Safety*, 58, 396–404.
- Ropel, L., Belvèze, L.S., Aki, S.N.V.K., Stadtherr, M.A., and Brennecke, J. (2005). Octanol-water partition coefficients of imidazolium-based ionic liquids. *Green Chemistry*, 7, 83–90.
- Schnepper, C. A. and Stadtherr, M. A. (1996). Robust Process Simulation Using Interval Methods. *Computers and Chemical Engineering*, 20, 187–199.
- Seydel, R. (1988). *From Equilibrium to Chaos: Practical Bifurcation and Stability Analysis*. New York, NY: Elsevier.
- Stepnowski, P., Skladanowski, A.C., Ludwiczak, A., and Laczynska, E. (2004). Evaluating the cytotoxicity of ionic liquids using human cell line HeLa. *Human and Experimental Toxicology*, 23, 513–517.

List of Figure Captions

Fig. 1. Bifurcation of equilibrium diagram for nutrient inflow concentration (x_n) versus inflow rate (D) in Canale's chemostat model. TE: Transcritical of equilibrium; FE: Fold of equilibrium; H: Hopf; H_p : Planar Hopf; FH: Fold- Hopf codimension-two. Region of stable coexistence shaded in grey.

Fig. 2. Solution branch diagram illustrating the change in equilibrium states (species biomass) with change in the nutrient concentration of the inflow (x_n) for Canale's chemostat model. From left to right: prey, predator, and superpredator biomasses. $D = 0.09$ for all three plots.

Fig. 3. Bifurcation of equilibrium diagrams for nutrient inflow concentration (x_n) versus contaminant concentration (C) in Canale's chemostat model with modified death rates given by Eq. (5). $D = 0.07$ for both plots. TE: Transcritical of equilibrium; FE: Fold of equilibrium; H: Hopf; H_p : Planar Hopf; FH: Fold-Hopf codimension-two. Regions of stable coexistence shaded in grey.

Fig. 4. Solution branch diagram illustrating the change in equilibrium states (species biomass) with change in the contaminant concentration (C) for Canale's chemostat model with modified death rates given by Eq. (5). From left to right: prey, predator, and superpredator biomasses. $D = 0.07$, $x_n = 200$, $C_1^{LC_{50}} = 10$, $C_2^{LC_{50}} = 100$, and $C_3^{LC_{50}} = 1000$ for all three plots.

Fig. 5. Bifurcation of equilibrium diagrams for nutrient inflow concentration (x_n) versus contaminant concentration (C) in Canale's chemostat model with modified death rates given by Eq. (5). $D = 0.07$ for both plots. TE: Transcritical of equilibrium; FE: Fold of equilibrium; H: Hopf; H_p : Planar Hopf; FH: Fold-Hopf codimension-two. Regions of stable coexistence shaded in grey.

Fig. 6. Solution branch diagram illustrating the change in equilibrium states (species biomass)

with change in the contaminant concentration (C) for Canale's chemostat model with modified death rates given by Eq. (5). From left to right: prey, predator, and superpredator biomasses. $D = 0.07$, $x_n = 200$, $C_1^{LC_{50}} = 1000$, $C_2^{LC_{50}} = 10$, and $C_3^{LC_{50}} = 100$ for all three plots.

Fig. 7. Bifurcation of equilibrium diagrams for nutrient inflow concentration (x_n) versus contaminant concentration (C) in Canale's chemostat model with modified death rates given by Eq. (5). $D = 0.07$ for both plots. TE: Transcritical of equilibrium; FE: Fold of equilibrium; H: Hopf; H_p : Planar Hopf; FH: Fold-Hopf codimension-two. Regions of stable coexistence not shown due to scale. See Fig. 8.

Fig. 8. Bifurcation of equilibrium diagram for nutrient inflow concentration (x_n) versus contaminant concentration (C) in Canale's chemostat model with modified death rates given by Eq. (5) and $D = 0.07$. TE: Transcritical of equilibrium; FE: Fold of equilibrium; H: Hopf; H_p : Planar Hopf; FH: Fold-Hopf codimension-two. Region of stable coexistence shaded in grey. See Fig. 7 for larger values of C .

Fig. 9. Solution branch diagram illustrating the change in equilibrium states (species biomass) with change in the contaminant concentration (C) for Canale's chemostat model with modified death rates given by Eq. (5). From left to right: prey, predator, and superpredator biomasses. $D = 0.07$, $x_n = 200$, $C_1^{LC_{50}} = 1000$, $C_2^{LC_{50}} = 100$, and $C_3^{LC_{50}} = 10$ for all three plots.

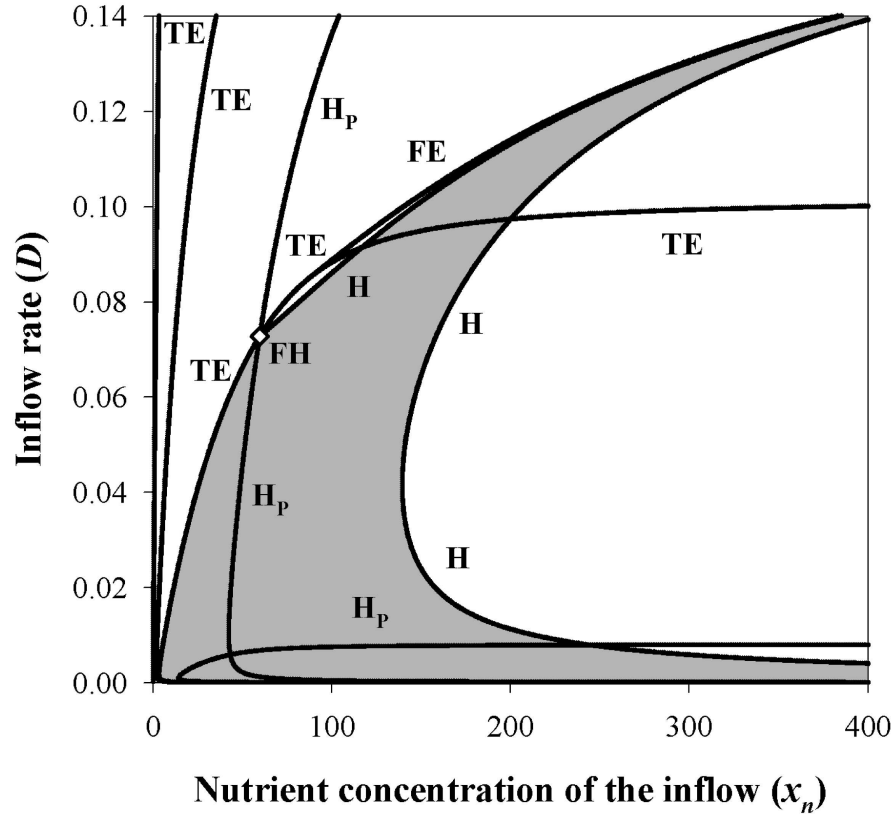


Figure 1: Bifurcation of equilibrium diagram for nutrient inflow concentration (x_n) versus inflow rate (D) in Canale's chemostat model. TE: Transcritical of equilibrium; FE: Fold of equilibrium; H: Hopf; H_p: Planar Hopf; FH: Fold- Hopf codimension-two. Region of stable coexistence shaded in grey.

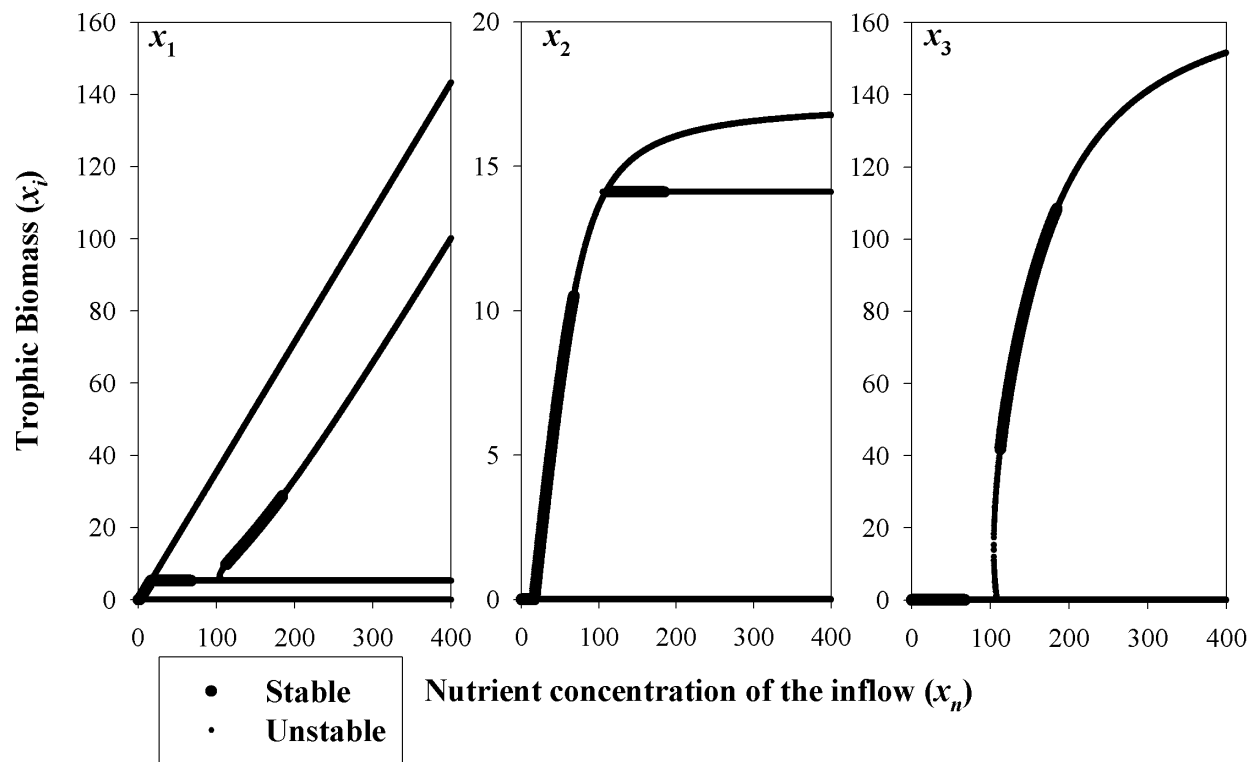


Figure 2: Solution branch diagram illustrating the change in equilibrium states (species biomass) with change in the nutrient concentration of the inflow (x_n) for Canale's chemostat model. From left to right: prey, predator, and superpredator biomasses. $D = 0.09$ for all three plots.

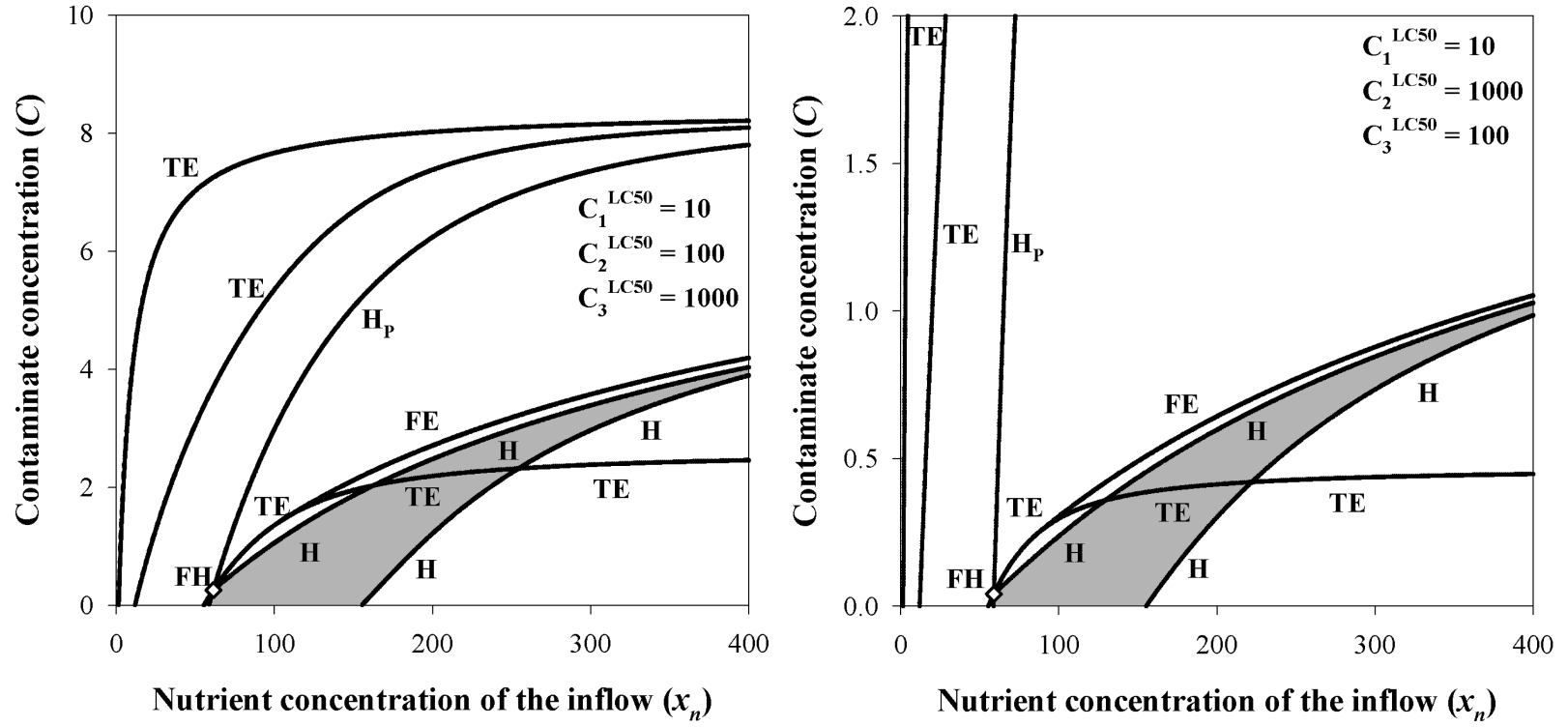


Figure 3: Bifurcation of equilibrium diagrams for nutrient inflow concentration (x_n) versus contaminant concentration (C) in Canale's chemostat model with modified death rates given by Eq. (5). $D = 0.07$ for both plots. TE: Transcritical of equilibrium; FE: Fold of equilibrium; H: Hopf; H_p: Planar Hopf; FH: Fold-Hopf codimension-two. Regions of stable coexistence shaded in grey.

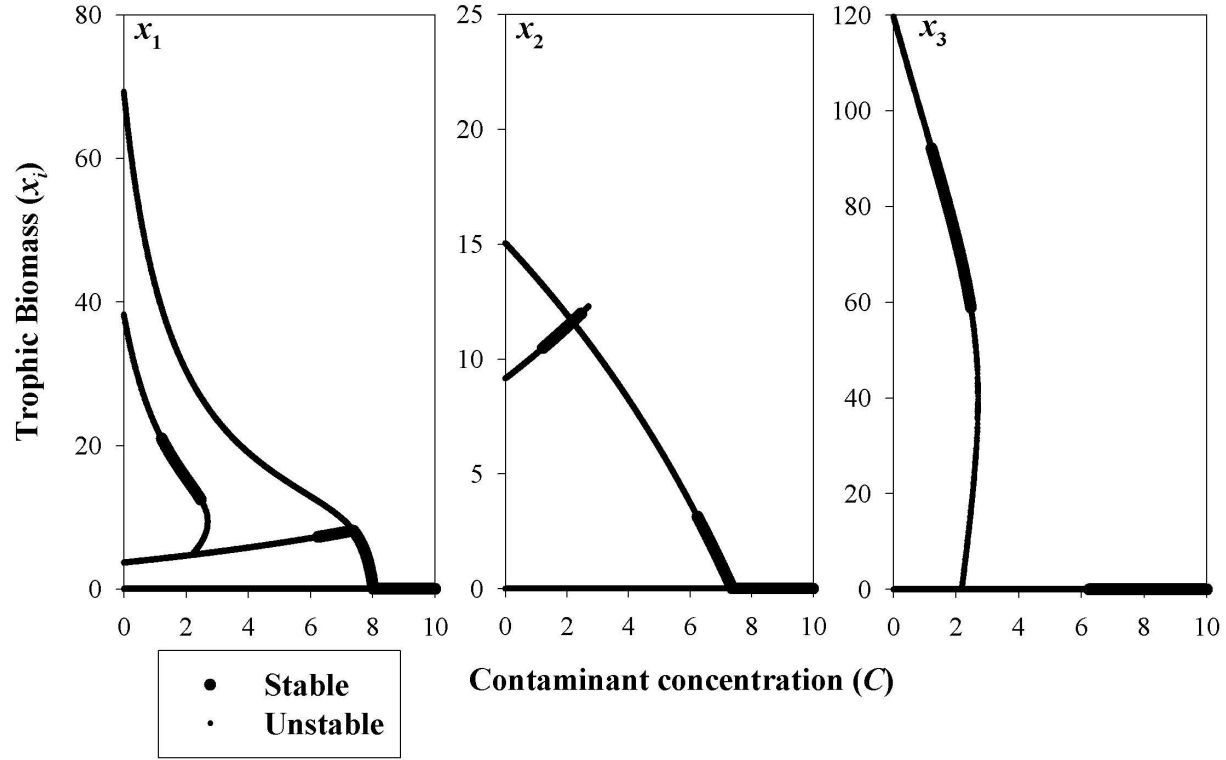


Figure 4: Solution branch diagram illustrating the change in equilibrium states (species biomass) with change in the contaminant concentration (C) for Canale's chemostat model with modified death rates given by Eq. (5). From left to right: prey, predator, and superpredator biomasses. $D = 0.07$, $x_n = 200$, $C_1^{\text{LC}_{50}} = 10$, $C_2^{\text{LC}_{50}} = 100$, and $C_3^{\text{LC}_{50}} = 1000$ for all three plots.

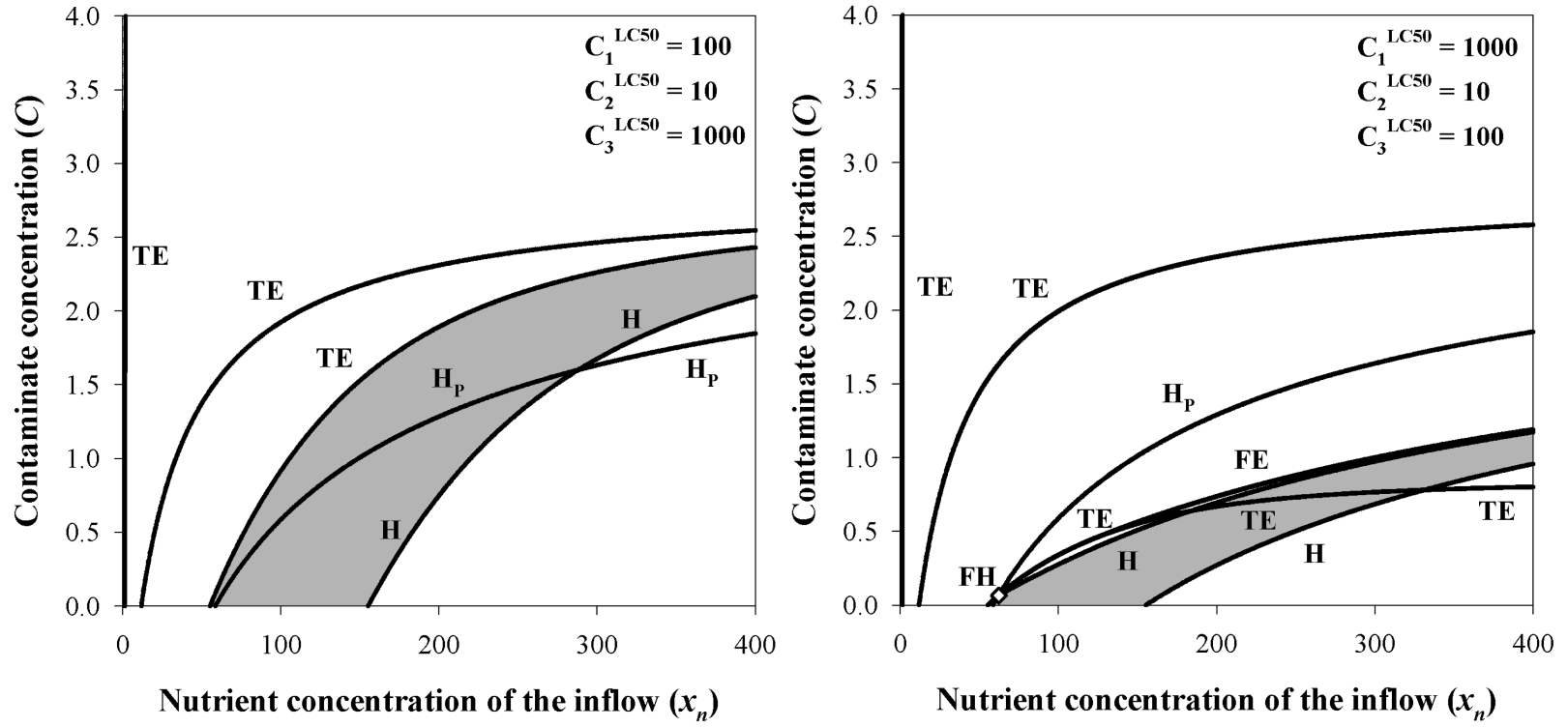


Figure 5: Bifurcation of equilibrium diagrams for nutrient inflow concentration (x_n) versus contaminant concentration (C) in Canale's chemostat model with modified death rates given by Eq. (5). $D = 0.07$ for both plots. TE: Transcritical of equilibrium; FE: Fold of equilibrium; H: Hopf; H_p : Planar Hopf; FH: Fold-Hopf codimension-two. Regions of stable coexistence shaded in grey.

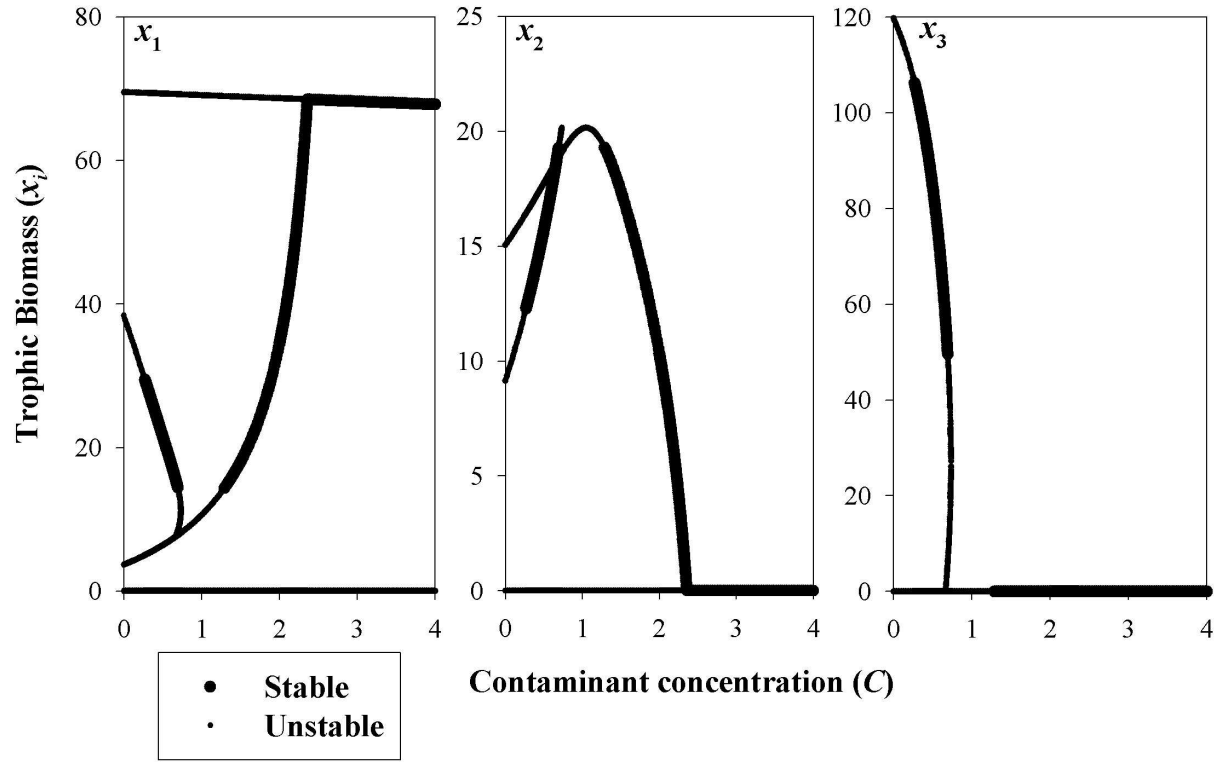


Figure 6: Solution branch diagram illustrating the change in equilibrium states (species biomass) with change in the contaminant concentration (C) for Canale's chemostat model with modified death rates given by Eq. (5). From left to right: prey, predator, and superpredator biomasses. $D = 0.07$, $x_n = 200$, $C_1^{\text{LC}_{50}} = 1000$, $C_2^{\text{LC}_{50}} = 10$, and $C_3^{\text{LC}_{50}} = 100$ for all three plots.

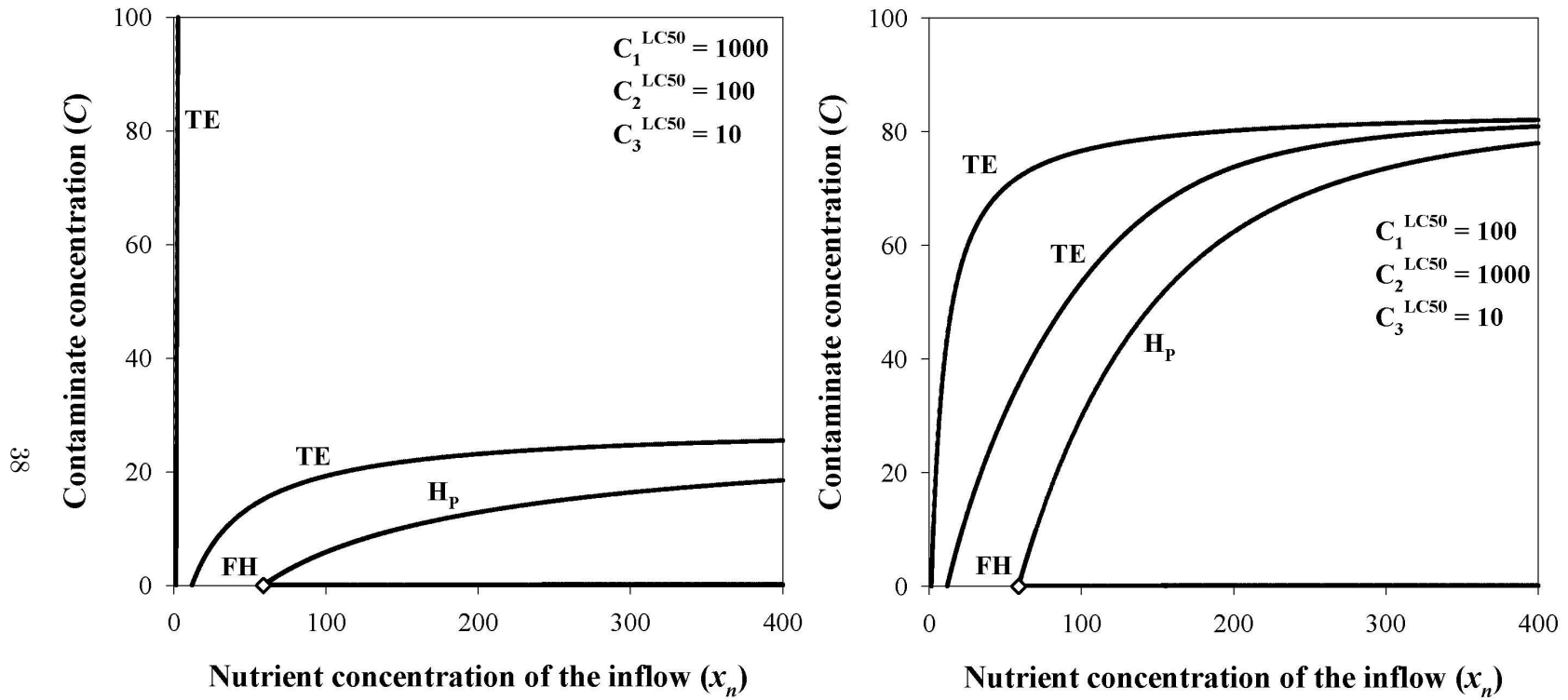


Figure 7: Bifurcation of equilibrium diagrams for nutrient inflow concentration (x_n) versus contaminant concentration (C) in Canale's chemostat model with modified death rates given by Eq. (5). $D = 0.07$ for both plots. TE: Transcritical of equilibrium; FE: Fold of equilibrium; H: Hopf; H_p: Planar Hopf; FH: Fold-Hopf codimension-two. Regions of stable coexistence not shown due to scale. See Fig. 8.

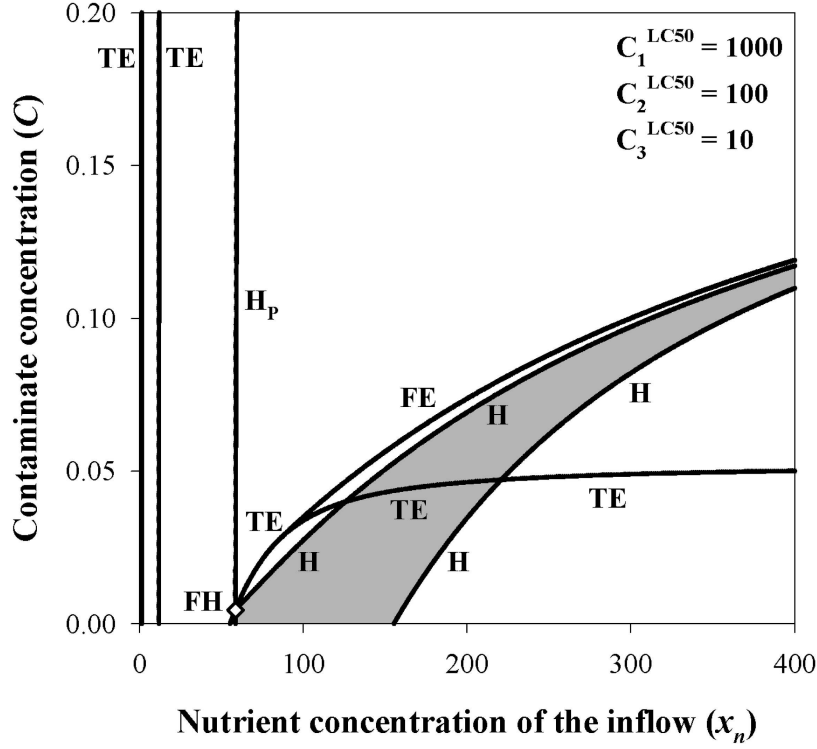


Figure 8: Bifurcation of equilibrium diagram for nutrient inflow concentration (x_n) versus contaminant concentration (C) in Canale's chemostat model with modified death rates given by Eq. (5) and $D = 0.07$. TE: Transcritical of equilibrium; FE: Fold of equilibrium; H: Hopf; H_p : Planar Hopf; FH: Fold-Hopf codimension-two. Region of stable coexistence shaded in grey. See Fig. 7 for larger values of C .

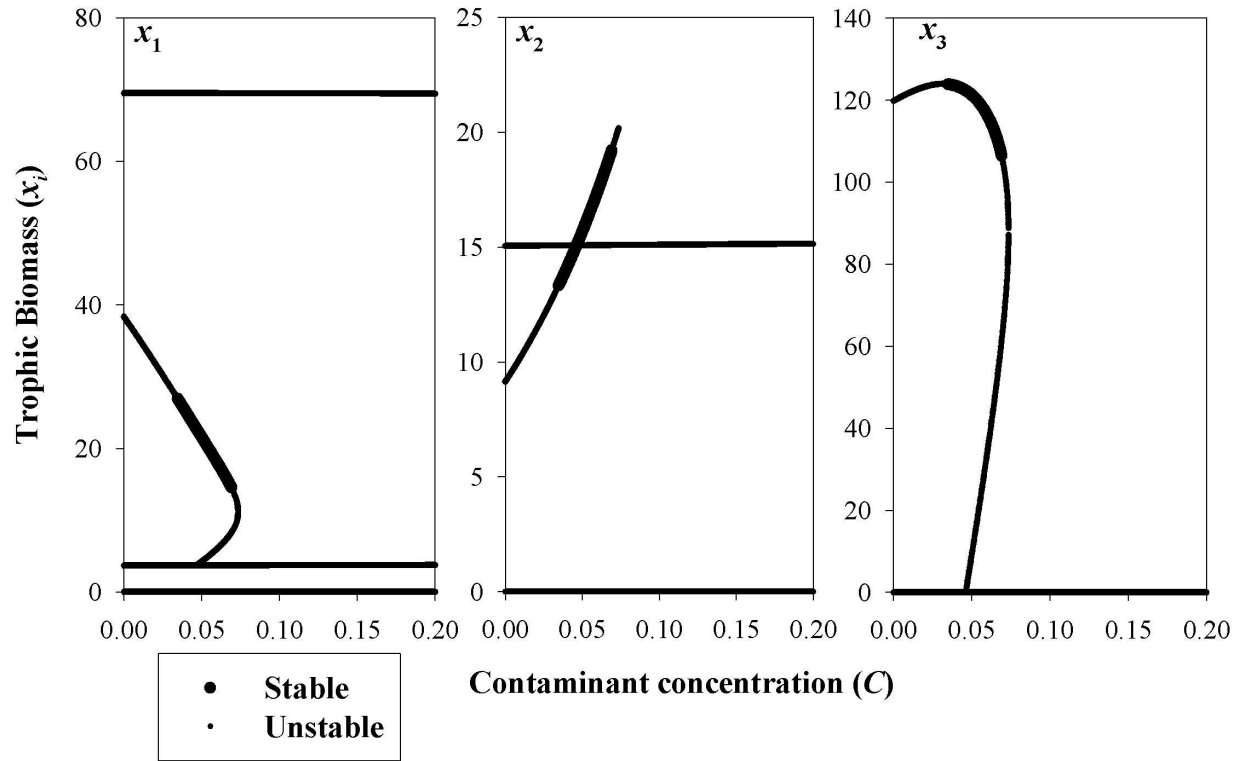


Figure 9: Solution branch diagram illustrating the change in equilibrium states (species biomass) with change in the contaminant concentration (C) for Canale's chemostat model with modified death rates given by Eq. (5). From left to right: prey, predator, and superpredator biomasses. $D = 0.07$, $x_n = 200$, $C_1^{\text{LC}_{50}} = 1000$, $C_2^{\text{LC}_{50}} = 100$, and $C_3^{\text{LC}_{50}} = 10$ for all three plots.